JOURNAL OF GEOPHYSICAL RESEARCH, VOL. 114, D00D07, doi:10.1029/2008JD011104, 2009

On the relationship between diurnal temperature range and surface solar radiation in Europe

Knut Makowski,[1] Eric B. Jaeger,[1] Marc Chiacchio,[1] Martin Wild,[1] Tracy Ewen,[1] and Atsumu Ohmura[1]

Received 4 September 2008; revised 17 December 2008; accepted 30 December 2008; published 8 April 2009.

[1] The surface solar radiation (SSR) is an important factor influencing the local and global energy budget. However, information on the spatial and temporal variation of SSR is limited. A more commonly available measure, which may provide such information, is the diurnal temperature range (DTR). In this study we analyze the relationship between DTR and SSR in Europe between 1970 and 2005 on seasonal and decadal scale. When comparing the mean anomalies time series composed of 31 pairs of sites with long-term SSR and DTR measurements, we found a correlation coefficient of 0.87 in the annual mean and between 0.61 and 0.92 in the seasonal mean anomalies. When investigating the individual pairs of SSR and DTR individually, we found that local correlations are mostly lower than the European mean and that they decrease rapidly in seasons and latitudes with low incident angles and at high alpine altitude. The highest correlation on local and seasonal scales seems to be connected with the variability of the large-scale circulation in Europe. The output of 11 simulations of current generation regional climate models over Europe confirms the strong relationship between SSR and DTR. The seasonal dependence of the relationship is well reproduced, but the absolute values of DTR and SSR are mostly too low. The pattern of decrease (dimming) and increase (brightening) in SSR and DTR was not reproduced in the modeled time series. There is still strong evidence from both models and observations that DTR is a reliable representative of SSR.

Citation: Makowski, K., E. B. Jaeger, M. Chiacchio, M. Wild, T. Ewen, and A. Ohmura (2009), On the relationship between diurnal temperature range and surface solar radiation in Europe, *J. Geophys. Res.*, *114*, D00D07, doi:10.1029/2008JD011104.

1. Introduction

[2] Observing and anticipating changes of complex climate variables such as downwelling surface solar radiation (SSR hereinafter) in the past and the future is not always straightforward and, yet, is of utmost importance. Sunshine recorders, radiometers or pyrheliometers require high maintenance and a sufficient infrastructure and knowledge to produce reliable output. Much of the technology that is used today to measure radiative fluxes, which determine the energy balance and therewith the temperature, has been available with sufficient quality for only a few decades around the globe.

[3] Measurements that can replace or approximate the lacking information are therefore highly desirable. A much more commonly available measure which may inherit a fingerprint of SSR is the diurnal temperature range (DTR) [*Makowski et al.*, 2008]. Until now only a few publications have highlighted the close connection between the diurnal temperature cycle and the SSR. In 1984 *Bristow and Campbell* [1984] already identified the need to obtain reliable SSR data. They reconstructed SSR using an empirical formula for three sites in the United States and emphasized that the relationship between DTR and SSR varies over the year, which should be taken into account.

[4] *Liu et al.* [2004] investigated a data set of daily maximum and minimum temperature, cloud cover, and SSR which covers most of China for a period of 45 years. They found a correlation coefficient between DTR and SSR as high as 0.88 in the annual mean anomalies. *Wild et al.* [2007] suggested a close correlation between long-term changes in SSR and DTR on a global basis. *Liu et al.* [2004] additionally show that changes in cloud cover were not the main cause for changes in the SSR and daily temperature range, whereas several studies that investigated various parts of North America found this to be the case [*Karl et al.*, 1984; *Plantico et al.*, 1990].

[5] As stated above, only a few studies compare DTR and SSR directly. For Europe, no work incorporating both measures has been published so far. Studies referring to one of the measures [e.g., *Dai et al.*, 1997] show that correlations between DTR and precipitation are as high as 0.55, whereas the correlation between DTR and total cloud cover is only 0.35. *Teuling et al.* [2009] show a close correlation between SSR and evaporation in the northerly part of Europe whereas in southern Europe SSR and precipitation are more closely correlated. This indicates that

[1]Institute for Atmospheric and Climate Science, ETH Zurich, Zurich, Switzerland.

0148-0227/09/2008JD011104$09.00

Table 1. Latitudes, Longitudes, Names, Identification Number, Country Codes, and Distances Between All Pairs of Sites of Diurnal Temperature Range and Surface Solar Radiation[a]

Identification Number	SSR Site	CTRY	Lat	Lon	DTR Site	CTRY	Lat	Lon	Dist, km
1171	Sonnblick	AT	47.00	12.95	Sonnblick	AT	47.00	12.95	6
1176	Uccle	BE	50.80	4.35	Uccle	BE	50.80	4.35	0
1179	St. Hubert	BE	50.00	5.40	Luxembourg Airport	LU	49.62	6.22	73
1189	Hradec Kralove	CZ	50.20	15.85	Praha-Klementinum	CZ	50.08	14.42	103
1203	Hamburg	DE	53.60	10.11	Hamburg Bergdorf	DE	53.48	10.25	16
1205	Braunschweig	DE	52.30	10.45	Hannover	DE	52.47	9.68	56
1216	Würzburg	DE	49.70	9.96	Würzburg	DE	49.77	9.97	8
1217	Trier	DE	49.70	6.66	Saarbrücken-Ensheim	DE	49.22	7.12	63
1224	Weihenstephan	DE	48.40	11.70	Augsburg	DE	48.43	10.93	57
1237	Sodankyla	FI	67.30	26.65	Sodankyla	FI	67.37	26.65	8
1238	Jokioinen	FI	60.80	23.50	Helsinki	FI	60.17	24.95	106
1246	Nancy-Essey	FR	48.60	6.21	Nancy	FR	48.67	6.20	8
1257	Limoges	FR	45.80	1.28	Déols-Chateauroux	FR	46.85	1.72	122
1264	Millau	FR	44.10	3.01	Mont-Aigoual	FR	44.12	3.58	46
1266	Nice	FR	43.60	7.20	Marseille	FR	43.30	5.38	151
1283	Eskdalemuir	GB	55.30	−3.20	Prestwick	GB	55.50	−4.58	90
1299	London, Weather C.	GB	51.50	−0.12	Oxford	GB	51.77	−1.27	85
1320	Budapest	HU	47.40	19.18	Hurbanovo	SK	47.87	18.20	90
1338	Reykjavik	IS	64.10	−21.90	Reykjavik	IS	64.13	−21.90	3
1381	De Bilt	NL	52.10	5.18	De Bilt	NL	52.10	5.18	0
1384	Bergen	NO	60.40	5.31	Flesland	NO	60.28	5.22	14
1386	Kolobrzeg	PL	54.10	15.58	Leba	PL	54.75	17.53	146
1389	Warszawa	PL	52.20	20.98	Siedlce	PL	52.25	22.25	87
1393	Zakopane	PL	49.20	19.96	Poprad-Tatry	SK	49.07	20.25	26
1412	Kiruna	SE	67.80	20.23	Kiruna	SE	67.82	20.32	4
1413	Lulea	SE	65.50	22.13	Haparanda	SE	65.82	24.12	98
1414	Stockholm	SE	59.30	17.95	Visby	SE	57.65	18.33	185
1420	Kyiv	UA	50.40	30.45	Kyiv	UA	50.40	30.53	6
1421	Odessa	UA	46.40	30.63	Sulina	RO	45.17	29.73	154
1438	Sljeme-Puntijarka	HR	45.90	15.96	Zagreb-Gric	HR	45.82	15.97	9
1479	Wien, Hohe Warte	AT	48.20	16.36	Wien, Hohe Warte	AT	48.23	16.35	3

[a]Latitudes, Lat; longitudes, Lon; distance, Dist; country codes, CTRY; diurnal temperature range, DTR; surface solar radiation, SSR.

moisture availability is not a limiting factor for evaporation in central and northern Europe and therefore should have a minor influence on DTR in those areas. Since moisture can have a strong impact on DTR [*Zhou et al.*, 2008] this is an important finding for our study.

[6] In the present work, we assess the relationship between SSR and the DTR in Europe on seasonal and decadal scales. The seasonal and decadal scale was used to reduce the strong short-term imprint of weather on the connection between SSR and DTR. We incorporate different types of data including measured station-based, measured gridded, and modeled. Since this article is a contribution to the special issue on global dimming and brightening we will refer to this issue at several points.

2. Data

[7] As stated above, the overall data can be divided into three groups: measured data on a station basis (DTR and SSR), gridded measured data (DTR) and gridded model data (DTR and SSR).

2.1. Station Data Sets

[8] The most sparsely available data type that we use in this study is the measured station SSR data. Therefore, we started by identifying as many sites as possible, according to the criteria given below, for the period 1970 until 2005 which is the period best covered by data (M. Chiacchio and M. Wild, Long-term seasonal variations of surface solar radiation in Europe, manuscript in preparation, 2009). In a second step, we identified stations that provided data for daily maximum and minimum for the same period. To provide a comparable data set of SSR and DTR we used only stations separated by at most 200 km. However, the mean distance between an SSR measurement site and the next DTR measurement site which we identified is only 59 km (Table 1).

2.1.1. Surface Solar Radiation Station Data

[9] The SSR data used in this study is obtained from the GEBA database which contains monthly values of energy balance components on a station basis [*Gilgen and Ohmura*, 1999]. After updating the GEBA database with information provided by the World Radiation Data Center, we identified, on an annual basis, all stations in Europe that met the following demands despite the standard quality procedures in GEBA. Each station with not more than five years of missing data between 1970 and 2005 was accepted. An annual value was accepted if not more than one month was missing. If one month was missing, it was filled by using a station climatology derived from the previous, complete years within the 1970 to 2005 period. For the calculation of seasonal data, the same stations were used for easier comparison between the annual and the seasonal time series. Seasons of SSR, as for all other data, were calculated as mean values of March, April, May (spring); June, July, August (summer); September, October, November (autumn); and December, January, February (winter). For the winter mean of 1970, for example, December 1970, January and

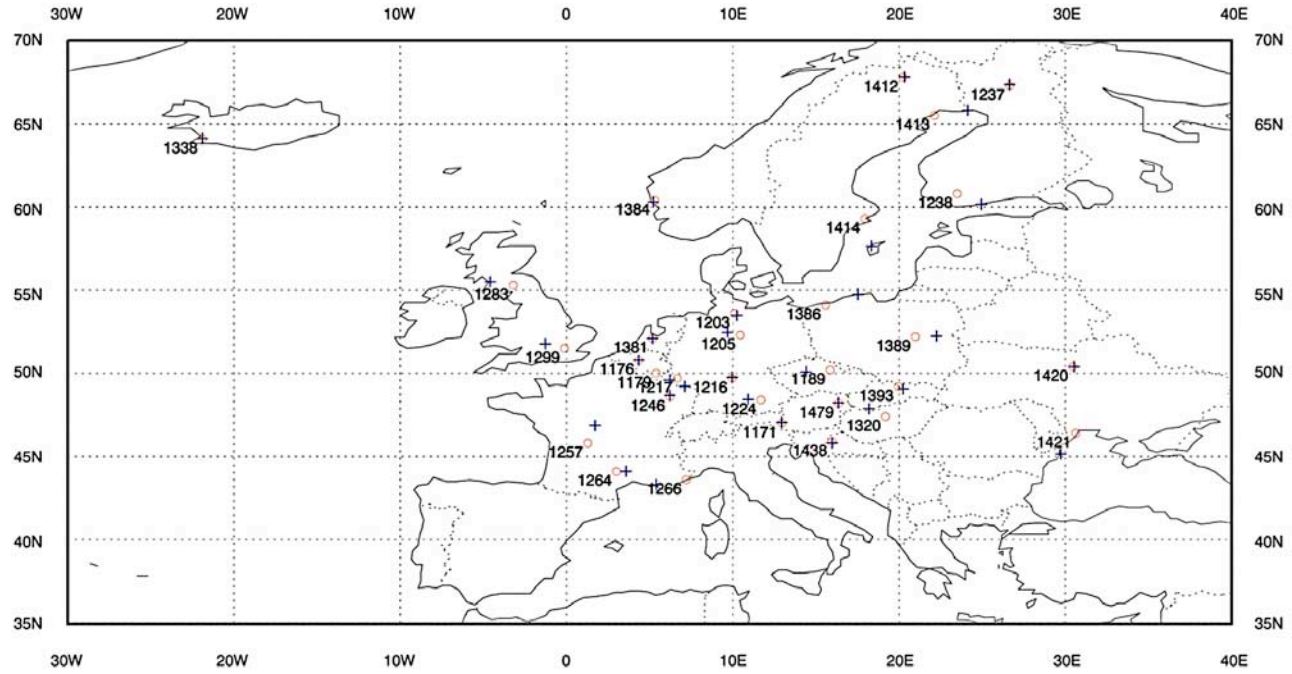

Figure 1. Map of all sites used in this study. Circles (red) show locations of the surface solar radiation (SSR) measurement site, and crosses (blue) show those of the sites measuring diurnal temperature range (DTR). The numbers represent the identification of each pair of stations (one DTR one SSR) as defined in Table 1.

February 1971 were used. Consequently, no winter for 2005 was calculated. No missing month was accepted for the calculation of the seasonal values. Following this analysis, 31 sites were identified which were suitable for the analysis (open circles, Figure 1). Although we have selected the sites used for this analysis most carefully, we cannot exclude the possibility that there remain some errors in the data. However, we believe that they do not have a substantial influence on the major outcomes of this study.

2.1.2. DTR Station Data

[10] Most of the DTR data used here originates from an earlier study; the retrieval procedure and qualitative criteria are given by *Makowski et al.* [2008]. The original source of the majority of the station DTR data used is the data set of the European Climate Assessment and Data Set (ECAD) project [*Klein Tank et al.*, 2002]. In addition to the data from *Makowski et al.* [2008], we included the following stations: Haparanda (also from the ECAD project), Sonnblick, Wien Hohe Warte, Bergen Flesland, Visby and Kiruna [from *Makowski*, 2006]. Finally, we obtained data from airport authorities at Prestwick via the commercial provider AWIS–Weather Services (crosses, Figure 1).

[11] For the calculation of the monthly means, no more than 10 missing days were accepted. For the annual means no missing months are accepted; if 1 month was missing it was filled by the mean of the previous and the consecutive year. If one of those was not available then the complete year was rejected. The absolute maximum of accepted filled months for a given year was three. In total, no more than 3 years missing for the selection of a station was accepted. However, only Prestwick has three missing years and Kiruna two missing years, whereas all other sites provide complete data or miss only 1 year in the annual time series.

2.2. DTR Gridded Data Sets

[12] We use two different gridded data sets to compare our results to. The CRU TS2.10 and the gridded data set from the European Union (EU) FP6 project ENSEMBLES. For both data sets we calculate the area weighted mean for the land area within 25°W to 35°E and 43°N to 68°N which is the same area cover by our DTR and SSR station data set (Figure 1).

2.2.1. CRU

[13] The data set CRU TS2.10 from the Climate Research Unit (CRU) of the University of East Anglia [*Mitchell and Jones*, 2005] provides monthly mean values for various measures for the global land area, including diurnal temperature range. The temporal coverage is 1901 to 2002 on a $0.5° \times 0.5°$ grid. Periods with missing data in the CRU data set are completed using climatology data from the 1961 to 1990 period. We removed, as far as possible, the data filled by climatology values according to the station information data set provided by CRU. From Figure 7 of *Mitchell and Jones* [2005] we found that since about 1990 the number of stations used to create the data set in the area of Europe and the former Union of Soviet Socialist Republics (USSR) varied considerably. For the area of Europe more than 550 stations were available from 1965 until 1985. Subsequently, the overall amount broke down to about 100 until the late 1990s when the number increases again up to 350 and declines again thereafter toward the end of the data set in 2002. For the area of the former USSR the development

Table 2. Abbreviations of Hosting Institutions Together With the Analyzed Resolutions and Models, and the Corresponding References Including the Model Descriptions

Institute	Model	Resolution	Reference
C4I22	RCA	25 km	*Jones et al.* [2004], *Kjellström et al.* [2005]
CNRM22	Aladin	25 km	*ALADIN International Team* [1997]
DMI22	HIRHAM	25 km	*Christensen et al.* [1996]
ETHZ22/ETHZ44	CLM	25 km/50 km	*Steppeler et al.* [2003]
ICTP22	RegCM	25 km	*Giorgi and Mearns* [1999], *Pal et al.* [2007]
KNMI22/KNMI44	RACMO	25 km/50 km	*Lenderink et al.* [2003]
MPI22	REMO	25 km	*Jacob et al.* [2001]
SMHI22	RCA	25 km	*Jones et al.* [2004], *Kjellström et al.* [2005]
OURANOS22	CRCM	25 km	*Plummer et al.* [2006]

of station availability is comparable. For the years between 1960 and the late 1980s the amount of available data in total stays rather constant and includes about 250 sites. During the early 1990s nearly no data are available. The number of available sites also increases thereafter but only up to 150 stations.

[14] We have described the development of data availability in the CRU data set in detail to illustrate that we had to be careful during our comparison with the measured data, which does vary only slightly in the amount of available data over time. We will refer back to this in the results sections.

2.2.2. ECAD

[15] The gridded data set from the EU-FP6 project ENSEMBLES is based on the data gathered in the European Climate Assessment and Data set Project. Subsequently, we will refer to this data set as the ECAD data set. This should not be confused with the DTR station data we used partly originating from the ECAD project. The ECAD data set [*Haylock et al.*, 2008] contains daily data between 1950 and 2006. We use the data with a spatial resolution of $0.5^\circ \times 0.5^\circ$ on the same regular grid as the CRU data set. The variables contained in the ECAD data set are daily mean temperature and daily precipitation as well as daily maximum and daily minimum temperature from which we calculated monthly means of DTR. Approximately 1000 stations were used in total for this data set. Prior to 1960 and after 2000 the number of stations is markedly lower (e.g., year 2000 about 1000 sites; year 2002 about 800 sites; year 2006 about 550 sites [see *Haylock et al.*, 2008, Figures 2 and 3]). On the basis of this, we restricted our analysis of this data set to the period 1970 until 2000.

2.3. Model Data

[16] We use monthly mean DTR and SSR fields from the regional climate models (RCMs) included in the EU-FP6 project ENSEMBLES (www.ensembles-eu.org). Most RCMs have three experiments available: a control simulation (CTL) for contemporary climate at 50-km and 25-km resolution (both for 1958–2001) and a transient simulation (1951 through 2050 or 2100) at 25-km resolution conducted for the European continent. The control simulations were all driven at the lateral boundaries using the ERA40 reanalysis [*Uppala et al.*, 2005], whereas the transient simulations use different GCM boundary conditions. Here, we focus only on the CTL simulations at 25km resolution. Additionally, for two RCMs the 50km simulations were used. We assess only those simulations that have been interpolated onto the regular CRU grid covering the European continent and parts of the North Atlantic. All analyses have been performed for Europe, excluding the Mediterranean, using land points only.

[17] The 11 RCM simulations analyzed in this study are detailed in Table 2. Since two simulations were performed with the same model, we use the institution name to unambiguously refer to a model version. Details on the model dynamics and physics or the simulation setups can be found on the ENSEMBLES homepage (www.ensembles-eu.org) or in the references given in Table 2.

3. Correlations and Trends in Annual and Seasonal Mean Anomalies

[18] In the following section and in section 4, we use observational data from stations and gridded data where measurements of daily maximum and minimum surface air temperature are available. With these measurements, the diurnal temperature range or amplitude is obtained and a comparison to the corresponding SSR data from the Global Energy Balance Archive (GEBA) [*Gilgen and Ohmura*, 1999] is made.

[19] We investigated the anomalies of DTR and SSR averaged (unweighted) over the European region. Anomalies were used to avoid potential biases caused by few missing measurements which occur especially in SSR.

3.1. Correlations of Mean Series of DTR and SSR

[20] In a first step of correlation calculations, we used the nondetrended anomalies time series of DTR and SSR as they are comparable to other studies, such as that of *Dai et al.* [1997], who showed a close correlation between DTR, precipitation, and clouds on a regional to continental scale. In addition, *Liu et al.* [2004] investigated the correlation of DTR and SSR in China. Upon comparing the two time series, strong correlations were found for the period 1970 to 2005 in the annual means (0.87), and also for the different seasons: spring (MAM): 0.88, summer (JJA): 0.92, autumn (SON): 0.88 and winter (DJF): 0.61 (Figures 2a–2e). All correlations are significant at the 99% level. It is clear that the higher the correlations, the bigger the influence of SSR on DTR; indeed the highest values can be found in summer, followed by spring and autumn. The annual mean correlation coefficient of 0.87 agrees well with the findings from *Liu et al.* [2004] in China and is substantially higher than the correlations between DTR and precipitation or cloud

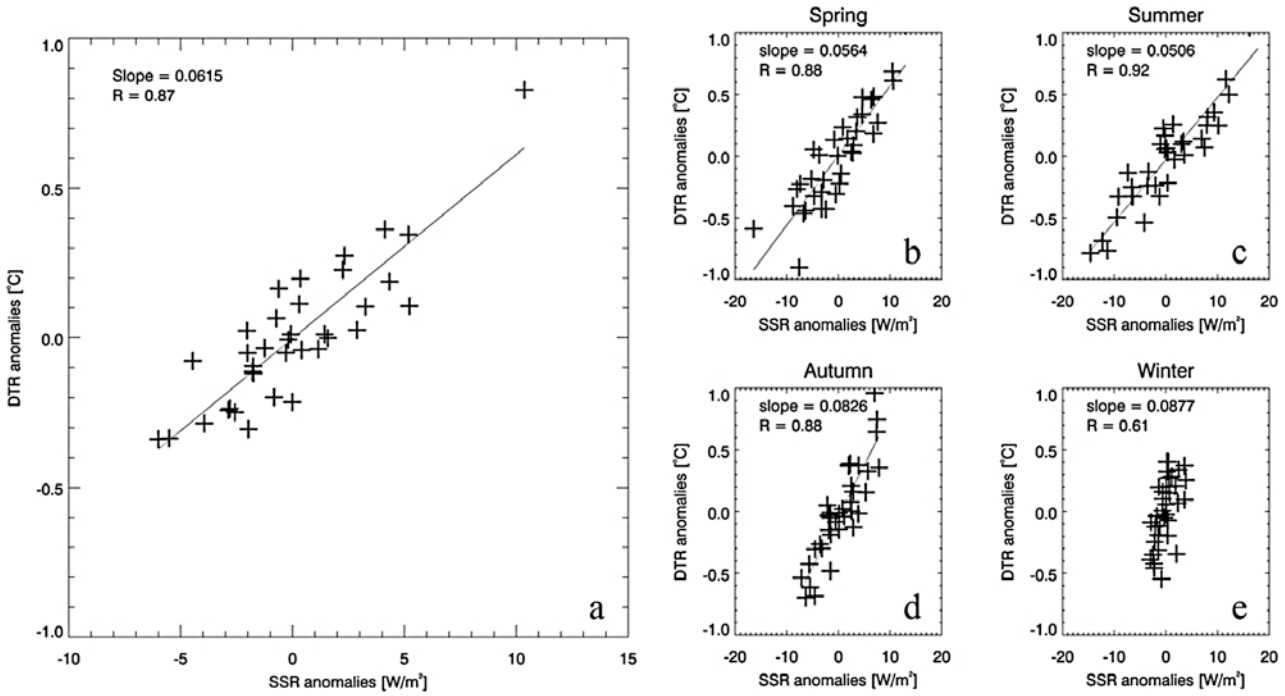

Figure 2. Scatterplots of anomaly means of the station data set of diurnal temperature range (DTR) and surface solar radiation (SSR). Plots include a best fit regression line and its slope as well as the corresponding correlation coefficient, (R). These plots are shown for (a) annual mean and (b–e) the different seasons. Note the different scales on the *x* axis.

cover as given by *Dai et al.* [1997]. The quality of the correlation is described by the correlation coefficient while the strength is described by the slope of the regression line. We found that with an increasing amount of SSR in the seasonal mean the slope changes (decrease). The change of the slope in the different seasons points to a not completely linear relationship between DTR and SSR (Figures 2b–2e). Potential causes for this nonlinearity may be changing hydrological conditions during the different seasons and the nonlinear relationship between radiation and temperature (i.e., the Stefan-Boltzmann law).

[21] In order to distinguish between the decadal and interannual agreement of the two measures, we detrended the mean time series and recalculated the correlations between the high (interannual variability) and the low (multiannual to decadal variability) frequency part of each series. To detrend the time series, a fit was determined by the robust locally weighted regression algorithm "Lowess" [*Cleveland*, 1979] and subtracted from the time series. The correlation coefficients for the detrended residuals or high-frequency changes in DTR and SSR are of the same magnitude as the raw time series, namely spring: 0.86, summer: 0.94, autumn: 0.88, winter: 0.61 and 0.89 for the annual mean. In contrast, the correlations of the low-frequency (smoothed) time series are substantially different. The best agreement in the low-frequency, long-term behavior could be found in spring (0.98), while all other seasons show correlation coefficients around 0.76. The correlation of the annual means is 0.49. All correlation coefficients are significant at 95%. This indicates that multidecadal changes have a substantial influence on DTR and SSR causing a close relationship between both measures.

3.2. Statistical Trend Analysis of European Mean Anomalies

[22] To assess the temporal development of each of the two measures more thoroughly in a statistical way a multi regression analysis was carried out using polynomial trend models from first- to fourth-order polynomials. Each coefficient was tested using a two-sided t-test. We refrained from testing the axis intersect since we are using anomalies which are distributed near zero by definition. We call a trend significant (at the 95% level) if all coefficients are significant at the certain level and the residuals show white noise (no autocorrelations in the residuals).

[23] The annual mean time series of SSR shows a significant trend of second order, decreasing from 1970 to 1985 and increasing thereafter (Figure 3a). This confirms the well known phenomenon of global dimming and global brightening [*Stanhill and Cohen*, 2001; *Liepert*, 2002; *Pinker et al.*, 2005; *Wild et al.*, 2005] in Europe. Though DTR is closely correlated to SSR it does not show a significant trend in any of the tested trend models. We consider the damping influence of factors like soil moisture, evaporation and clouds as most likely reasons which have led to the weakened, long-term trend development.

[24] On a seasonal scale the DTR time series of spring shows a significant increasing linear trend. The trend is mirrored in the SSR time series but is only significant at the 90% level (Figure 3b). In summer and autumn SSR development again can be approximated by a second-order

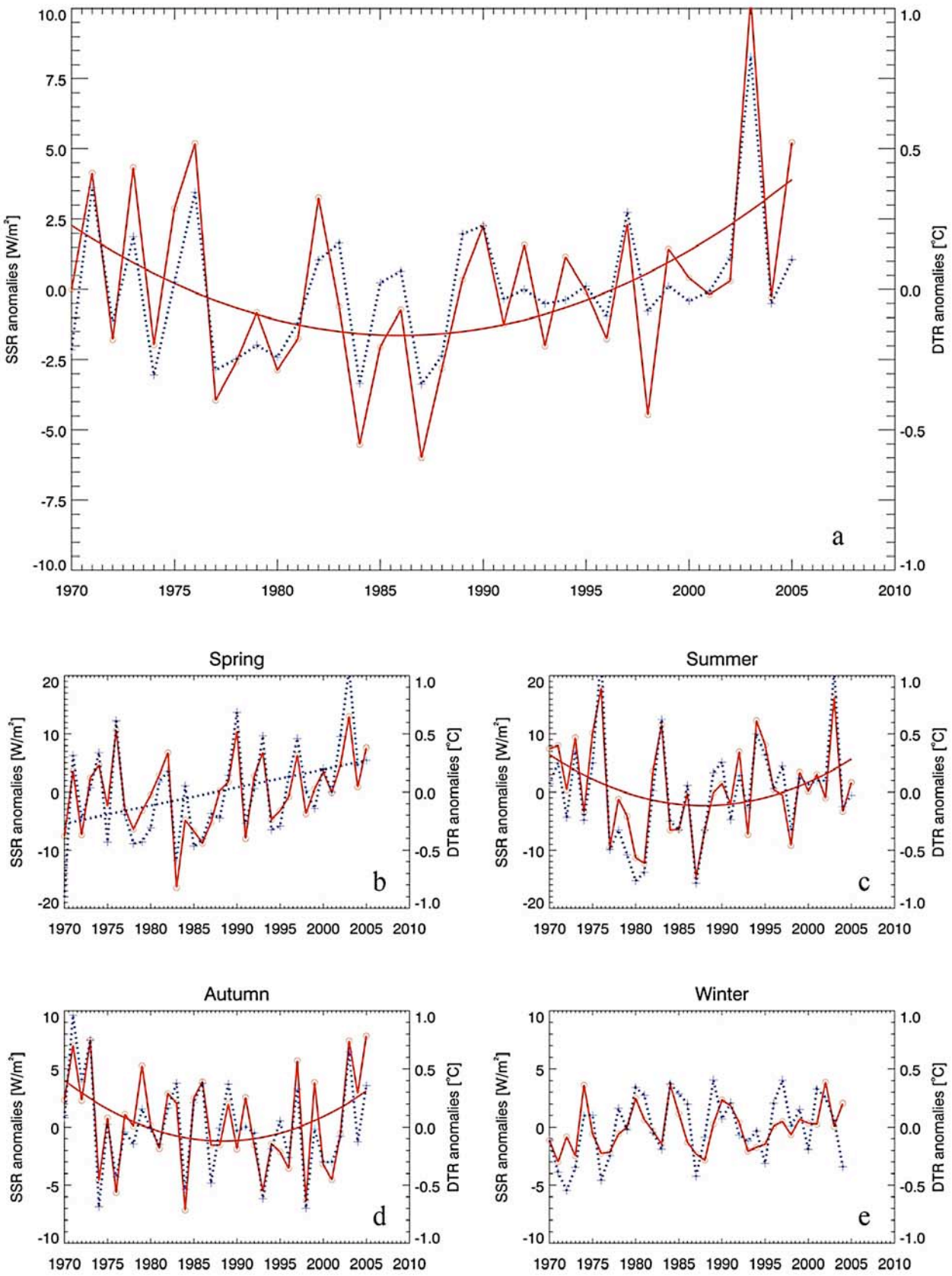

Figure 3. Times series plots of anomalies averaged over the station data set of diurnal temperature range (DTR, dashed blue with crosses) and surface solar radiation (SSR, solid red with circles). Plots include the best fit trend model between first- and fourth-order polynomial if the trend is significant at the 95% level.

Table 3. Correlation Coefficients as Derived From the Comparison Between ECAD and CRU Gridded Data Set Time Series of Diurnal Temperature Range With Station Data Set Diurnal Temperature Range and Surface Solar Radiation[a]

	Annual		Spring		Summer		Autumn		Winter	
	DTR	SSR	DTR	SSR	DTR	SSR	DTR	SSR	DTR	SSR
Original										
ECAD 2000	**0.94**	**0.87**	**0.65**	**0.72**	**0.82**	**0.84**	**0.75**	**0.58**	**0.83**	**0.48**
CRU 2002	**0.71**	**0.50**	**0.55**	**0.51**	**0.65**	**0.62**	**0.60**	**0.45**	**0.69**	0.33
CRU 1990	**0.83**	**0.62**	**0.62**	**0.53**	**0.81**	**0.78**	**0.67**	**0.56**	**0.75**	0.32
Short Term										
ECAD 2000	**0.94**	**0.89**	**0.62**	**0.72**	**0.79**	**0.85**	**0.74**	**0.55**	**0.89**	**0.49**
CRU 2002	**0.77**	**0.57**	**0.56**	**0.53**	**0.63**	**0.61**	**0.60**	**0.43**	**0.68**	0.27
CRU 1990	**0.87**	**0.72**	**0.57**	**0.50**	**0.78**	**0.80**	**0.76**	**0.61**	**0.75**	0.32
Long Term										
ECAD 2000	**0.67**	**0.87**	**0.97**	**0.78**	**0.97**	**0.88**	**0.92**	**0.95**	**0.71**	**0.57**
CRU 2002	−0.14	0.31	**0.62**	**0.61**	**0.59**	**0.81**	**0.88**	**0.94**	**0.79**	**0.80**
CRU 1990	**0.83**	0.41	**0.90**	**0.81**	**0.95**	**0.79**	0.20	0.05	**0.89**	**0.83**

[a]Diurnal temperature range, DTR; surface solar radiation, SSR. "Original" denotes coefficients for the original anomalies time series; "Short Term" denotes the remaining high-frequency, interannual variations after detrending with the Lowess algorithm; and "Long Term" denotes the correlations of the low-frequency part of the original time series as derived from Lowess. Coefficients given in bold are significant at the 95% level.

polynomial, in both cases DTR trends show similar behavior but miss the required significance level of 95% (Figures 3c and 3d). The trends for SSR are in line with Chiacchio and Wild (manuscript in preparation, 2009). Since we used a smaller subset of the GEBA data set, we are able to extend the analysis of our time series up to 2005. It confirms an ongoing of the brightening trend in the annual mean of SSR, as is also the case, and most pronounced, in the summer season. For further discussion of the possible mechanisms which may have led to the observed development of SSR we refer to Chiacchio and Wild (manuscript in preparation, 2009). Concerning DTR trends, we found no continuous decrease in any of the seasons or the annual mean, unlike many DTR observations around the globe which show a decrease between 1950 and the 1980s [*Karl et al.*, 1984, 1991, 1993; *Jones*, 1995; *Easterling et al.*, 1997]. In contrast, we found evidence for an ongoing increase of DTR, most dominant in spring, summer and autumn, which confirms our earlier findings on the annual mean trends in different regions in Europe [*Makowski et al.*, 2008].

3.3. Representativeness of the Station Data Sets for Europe

[25] In this section we investigate the representativeness of our 31 point sources of information by comparing them to gridded observational data sets of the Climate Research Unit of the University of East Anglia [*Mitchell and Jones*, 2005] and the recently published ENSEMBLES data set [*Haylock et al.*, 2008]. The purpose of this section is to assess the generality of our findings from the means of 31 point measurements for the general area of northern and central Europe.

[26] We calculated the area weighted mean series for ECAD and CRU for the domain within 25°W to 35°E and 43°N to 68°N, which is equivalent to the area which includes all 31 measurements. In general we found good agreement between the mean anomalies on an annual basis (Table 3 and Figure 4). Besides the calculation of the correlation coefficient for the "raw," measured anomaly data we have again split the time series into their high- and low-frequency parts by applying a Lowess algorithm [*Cleveland*, 1979] as described above. In Table 3, we compiled the correlation coefficients between the anomaly series of the DTR station data set (annual and seasonal), the ECAD data set (1970–2000) and the CRU data set (1970–2002 and 1970–1990) respectively. For the comparison with the CRU data set we used different periods to show the strong difference which occurs owing to the change in data availability of CRU (for details see section 2). For the comparison between ECAD DTR and station data set DTR we used the period 1970–2000 (see section 2).

[27] In all cases the correlations between the DTR station data set mean and ECAD were higher than if compared to CRU. This is equally true for the comparison of the unfiltered anomaly time series and also for the detrended high-frequency variations. The mean difference between the correlation coefficients of the original time series and the detrended high-frequency variations is about 0.03. The differences are consequently negligible, which shows that the interannual variations are strongly correlated and neither disturbed nor dependant on any low-frequency agreement in the compared time series. To reduce the overall information we focus on the detrended (high frequency; Table 3, rows 4–6) and long-term (low frequency; Table 3, rows 7–9) variability correlations for the rest of this section.

3.3.1. Agreement of the High-Frequency, Detrended Mean Series

[28] The correlation coefficient between annual mean DTR of CRU and the station data set DTR is only 0.77. However, when comparing only the 1970–1990 period it increases to 0.87. The difference originates from an inhomogeneity in the time series due to an abrupt change in data availability in the CRU data set since 1990 (Figure 4) as described in *Mitchell and Jones* [2005]. The ECAD data set

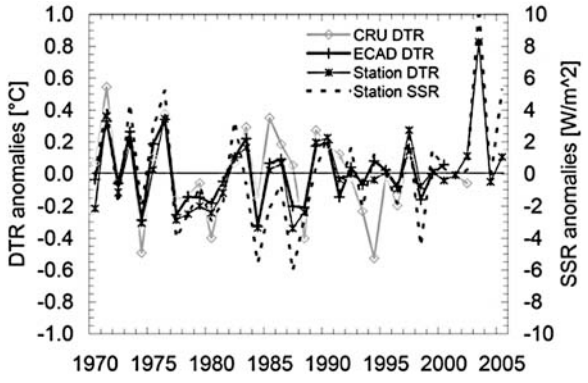

Figure 4. Anomaly time series from 1970 to 2005 of the ECAD (bold solid black line with crosses) and CRU (bold, solid gray line with diamonds) gridded data set (area weighted mean of: 25°W/35°E and 43°N/68°N) and station data set anomaly series of diurnal temperature range (DTR, thin black line with asterisk) and surface solar radiation (SSR, dashed line).

Table 4. Correlation Coefficients (Pearson) of Diurnal Temperature Range and Surface Solar Radiation[a]

Identification Number	Coefficients of Detrended Time Series Residuals					Coefficients of the Low-Frequency, Long-Term Variability of the Time Series[b]				
	Spring	Summer	Autumn	Winter	Annual	Spring	Summer	Autumn	Winter	Annual
All mean	**0.86**	**0.94**	**0.88**	**0.61**	**0.89**	**0.98**	**0.75**	**0.77**	**0.77**	**0.49**
1171	0.21	0.33	0.33	**−0.40**	0.35	**0.86**	**0.86**	**−0.80**	**0.95**	**0.73**
1176	**0.83**	**0.75**	**0.78**	**0.48**	**0.69**	**0.39**	**0.77**	**−0.47**	**−0.88**	**−0.36**
1179	**0.74**	**0.76**	**0.82**	0.23	**0.71**	0.14	**0.58**	0.09	**−0.79**	−0.25
1189	**0.75**	**0.74**	**0.77**	**0.37**	**0.75**	**0.63**	**0.86**	**0.36**	**0.85**	**0.45**
1203	**0.67**	**0.95**	**0.71**	0.07	**0.69**	**0.90**	**0.95**	**0.86**	0.23	**0.85**
1205	**0.74**	**0.94**	**0.73**	**0.50**	**0.83**	**−0.83**	−0.14	0.22	0.12	**−0.92**
1216	**0.83**	**0.87**	**0.90**	**0.79**	**0.89**	**0.37**	**0.96**	**0.90**	**0.78**	**0.88**
1217	**0.83**	**0.67**	**0.89**	**0.58**	**0.68**	**0.94**	**0.82**	**0.86**	0.10	**0.92**
1224	**0.65**	**0.63**	**0.80**	**0.63**	**0.65**	**0.79**	**0.60**	0.28	**0.50**	**0.43**
1237	**0.62**	**0.90**	**0.71**	−0.01	**0.64**	−0.31	**0.96**	**0.63**	**0.36**	0.26
1238	**0.70**	**0.65**	**0.39**	**0.36**	**0.61**	**0.71**	**0.74**	**0.87**	**0.91**	**0.70**
1246	**0.82**	**0.83**	**0.90**	**0.49**	**0.80**	**0.82**	**0.63**	**0.96**	0.32	**0.53**
1257	**0.86**	**0.83**	**0.83**	**0.55**	**0.70**	**0.77**	0.17	**0.88**	−0.17	**0.62**
1264	**0.80**	**0.66**	**0.71**	**0.77**	**0.69**	**0.70**	0.23	**0.46**	−0.03	−0.04
1266	**0.53**	**0.43**	**0.43**	**0.70**	**0.56**	**0.75**	**0.53**	**0.80**	**0.52**	**0.69**
1283	**0.70**	**0.74**	**0.51**	**0.43**	**0.53**	**0.79**	**0.83**	0.02	**0.72**	**0.53**
1299	**0.86**	**0.94**	**0.79**	**0.50**	**0.90**	**0.71**	**0.83**	**0.89**	**0.81**	**0.71**
1320	**0.72**	**0.58**	**0.75**	**0.56**	**0.70**	**0.87**	**−0.93**	**0.94**	**0.53**	**−0.77**
1338	**0.74**	**0.68**	**0.39**	0.18	**0.48**	0.04	**−0.95**	−0.31	−0.05	**−0.78**
1381	**0.80**	**0.87**	**0.77**	**0.75**	**0.73**	**0.83**	**0.78**	**0.90**	0.27	**0.81**
1384	**0.76**	**0.74**	**0.43**	**0.63**	**0.55**	0.11	**0.83**	−0.32	**0.41**	**0.34**
1386	**0.50**	**0.85**	**0.62**	**0.62**	**0.64**	0.09	−0.04	**0.64**	**0.69**	**−0.78**
1389	**0.61**	**0.76**	**0.79**	**0.67**	**0.58**	**0.62**	**0.73**	**0.78**	**0.73**	**0.66**
1393	**0.61**	**0.90**	**0.54**	**0.71**	**0.70**	0.02	**0.68**	0.13	**0.86**	0.16
1412	0.34	**0.90**	**0.51**	0.08	**0.50**	**−0.73**	**0.94**	**0.53**	**0.78**	**0.75**
1413	**0.72**	**0.66**	**0.52**	0.07	**0.62**	**0.38**	**0.91**	−0.26	**0.73**	**0.54**
1414	**0.65**	**0.70**	**0.48**	**0.48**	**0.49**	**0.95**	**0.97**	**0.56**	**0.66**	**0.96**
1420	**0.49**	0.32	**0.51**	**0.70**	0.20	**−0.39**	0.15	**0.88**	**0.77**	**0.69**
1421	**0.50**	0.25	**0.41**	**0.54**	**0.37**	**0.81**	**0.39**	**0.54**	**0.96**	**0.59**
1438	**0.67**	**0.59**	**0.44**	**0.60**	**0.65**	**−0.67**	**−0.89**	0.01	**−0.85**	**−0.95**
1479	**0.65**	**0.72**	**0.79**	**0.61**	**0.65**	**0.87**	**0.84**	**0.37**	**0.87**	**0.88**

[a]Identification gives information on the correlated pair of diurnal temperature range and surface solar radiation sites as defined in Table 1. Bold numbers are significant at 95% level.
[b]Determined with the Lowess algorithm.

series shows a higher correlation with the annual mean anomaly series of the station data set of 0.94 (Table 3, column 1, rows 4–6).

[29] We also compared the DTR time series from CRU and ECAD against the time series of the station data set SSR on annual and seasonal scales. In general we found lower agreement in all seasons between the station data set SSR and DTR from CRU and ECAD compared to the results from station data set DTR and SSR. However, the highest correlations were found in summer, 0.85 (SSR versus ECAD), 0.61 (SSR versus CRU 1970–2002) and 0.80 (SSR versus CRU 1970–1990).

[30] In comparing the annual mean anomalies of SSR against the two time series of the gridded data sets, we found differing results. The annual coefficients of the two CRU periods investigated were lower than those of corresponding summer season, namely 0.57 for SSR versus CRU, 1970–2002, and 0.72 for SSR versus CRU, 1970–1990. For the comparison of ECAD DTR against the station data set SSR we found a correlation coefficient of 0.89, which is exactly the same result as from the comparison of the two station data sets (Table 4, row 1).

3.3.2. Agreement in the Low-Frequency Component of Annual and Seasonal Means

[31] The correlations in the long-term variability of the average time series of the station data set DTR and SSR and the means derived from ECAD and CRU are in general high and significant. This shows that not only the high-frequency characteristics can be captured with as few as 31 sites, but also the lower-frequency variability (Table 3, rows 7–9).

[32] The most remarkable feature of the investigation on the low frequency is the strong disagreement between annual mean DTR of CRU 1970–2002 and the station data sets of DTR and SSR. However, when looking at the shorter period of CRU (1970–1990) it is obvious that it is not a disagreement due to a lack of a physical connection, but rather a data homogeneity issue as described above (section 2.2.1).

[33] It is noteworthy that the values of the mean time series of DTR derived from ECAD and CRU differ by only 0.1°C, whereas the station data set DTR series is on average 0.5°C lower than CRU and consequently 0.6°C lower than the ECAD time series. This bias is potentially due to the low station density in our station data set in southeast Europe where annual mean DTR values as high as 10°C occur.

[34] In summary, we found better agreement between our station data set DTR and SSR with the recently published ECAD data set than with the CRU data set. Since the ECAD data set is focused especially on Europe and has been developed with at least 20% more station data, we are

confident that it is more reliable for the investigated area. The high correlations between ECAD and the station time series which we use in this study underline that the results we obtained from our station series are representative of not only 31 locations, but of the overall domain which we investigated.

4. Local Comparison of Long- and Short-Term Variability

[35] In addition to looking at the correlations in the different seasons, we also compared each individual pair of stations (Table 1 and Figure 1) to gain information on spatial patterns. To distinguish between long- and short-term (interannual) agreements, we divided the original time series again into the high- and low-frequency components by detrending them with a Lowess filter. In the following sections we first take a look at the high-frequency variations before discussing the long-term variability.

4.1. Correlations of Local, Detrended Time Series of DTR and SSR

[36] The results are compiled in the left hand side (columns 2–6) of Table 4. The comparison shows that, in general, the correlations of the detrended European mean time series (nondetrended show in Figures 2 and 3) are higher than those of individual sites correlated with each other. This is a reasonable result since the averaging over the whole region smoothes out any locally disturbing influences such as advection of cold or warm air masses. Nevertheless, only few seasons for some sites miss the level of significant correlation as shown in Table 4 (all correlations significant above the 95% level are marked in bold font). More than one missing significant season can be found only at the stations 1171 (Sonnblick/Sonnblick (AT)) and 1412 (Kiruna/Kiruna (SE)).

[37] The pair 1171 is measured at the Austrian Observatory Sonnblick at an altitude of 3106 m (a.s.l.). All seasonal correlation coefficients show low values; during winter it is even significantly negative at the 95% level. At this altitude several reasons lead to a much lower correlation of DTR and SSR throughout the year. The absence of a stable boundary layer leads to a strong influence of well mixed, advected air masses. The height leads to much reduced cloud coverage and the snow cover, almost annual, leads to a high albedo. The lack of horizontal land area at this high-altitude station, which could receive the energy from the sun, changes the energetic behavior of the surrounding area. All factors are most intense during the period of low insolation, leading to the nonsignificant low or even negative correlation coefficients.

[38] Kiruna, where the station pair 1412 is measured is not located at high altitude yet at high latitude. The low-correlation coefficients in the short-term variations are occurring during winter and spring. Since the site receives rather small amounts of sunlight the variability is also rather low leading to lower correlations.

[39] The consequence of low insolation combined with sites located at high latitudes on the relationship between DTR and SSR can also be seen in the pairs 1237 (Sodankyla-FI), 1338 (Reykjavik-IS) and 1413 (Haparanda-SE), all of which are located north of 65°N, and show a non significant correlation coefficient in the winter season.

4.2. Correlations of Local, Long-Term Characteristics

[40] In this section we will assess the correlations between the low-frequency or long-term variability of the individual station pairs as defined in Table 1. Looking at the right hand side of Table 4 (columns 7–11) it is obvious that the time series agree less in their lower-frequency fraction. This behavior is partly explainable by the different nature of the high- and low-frequency part of the time series. The individual points of the high-frequency component of a seasonal series are determined with a gap of 9 months in between (the seasonal mean consists of 3 months), which leads to the absence of autocorrelations between the various data points. The low-frequency part is by definition derived from more than one consecutive point. Consequently each point contains information from the surrounding points. This leads to a much more persistent, disturbing influence of a potential erroneous outlier on the correlation of the long-term changes between the DTR and SSR series. Taking this into account we will subsequently only discuss the substantial results and discrepancies.

[41] The results of the long-term correlations are more heterogeneous compared to those of the high-frequency analysis. Two thirds of all correlated averaging periods show significant positive correlation. The correlation coefficients of the overall mean series are not generally the highest, still all are significantly positive. It is noteworthy that among the overall means the long-term variations of the seasons have higher correlations than the annual mean. Summarizing the individual averaging periods of the station pairs, only 8 out of the 31 pairs are not significant or negatively correlated during the summer season, which underpins the close relationship between DTR and SSR in the season with the highest amount of radiation.

[42] The station pairs with the largest discrepancies (3 or 4 of the seasonal means not significant or negatively correlated) in the correlation of long-term variability are 1179 (St. Hubert/Luxemburg Airport), 1205 (Braunschweig/Hannover), 1338 (Reykjavik/Reykjavik (IS)) and 1438 (Sljeme-Puntijarka/Zagreb-Gric (HR)) (Table 4).

[43] Sljeme-Puntijarka (SSR of 1438) and Zagreb-Gric (DTR of 1438) are separated by a horizontal distance of only 9 km. The difference in height is also negligible. Still this pair shows no significant correlation in any of the investigated seasons or the annual mean is instead significantly negative. When comparing the series of DTR and SSR of the station pair 1438 to the closest located pairs we found that prior to 1985 the series of SSR at 1438 shows an extraordinary behavior (increase followed by a steep decrease; series not shown) compared to those of 1479 and 1320 (although not the case for 1171, for the reasons stated below). This is evident in all seasons and subsequently in the annual mean series. As a further check, we recalculated all correlations beginning from 1985 which resulted in a significant increase of the long-term correlation coefficients; spring: 0.80/−0.67 (now/before), summer: 0.75/−0.89, autumn: 0.42/0.01, winter: 0.91/−0.85 and in the annual mean: 0.55/−0.95. These results refer to only 20 years of data but still they indicate that more of an inhomogeneity issue rather than a physical process might

explain the low and nonsignificant correlation between DTR and SSR at 1438.

[44] The pair 1338 (Reykjavik/Reykjavik), which is the second station pair with 4 nonsignificant or negative correlated seasons in the long-term analysis (Table 4), is located close to the Arctic Circle and at the coast of an island. On the one hand, this leads to an intense maritime and advective influence, and on the other hand, to a low imprint of SSR due to low insolation angles in all seasons, most intensely during the winter period in the Northern Hemisphere.

[45] The last two pairs with at least three nonsignificant or negatively correlated seasons are: 1179 (St. Hubert/Luxemburg Airport) and 1205 (Braunschweig/Hannover). All four measurement series (of DTR and SSR) show no extraordinary long-term trend behavior and no indication of data inhomogeneities. Also their geographical location is not at a high altitude or latitude or very close to the sea. The only potential influencing factor is the distance between the DTR an SSR sites which is in both cases more than 50 km. Since there are many other station pairs with an equal or higher horizontal distance which are strongly correlated, this is not necessarily the explanation from the strong disagreement. Consequently further investigations are needed.

4.3. Influence of the Large-Scale Circulation on the Long- and Short-Term Agreement Between DTR and SSR

[46] The geographical overviews given in Figure 5 show the values of the highest-correlation coefficients of all seasons and the season in which they occurred (indicated with colored symbols). Figure 5a gives the distribution of the highest-correlation coefficients of the detrended short-term variations, while Figure 5b shows those for the low-frequency parts of the DTR and SSR time series. The symbols are smaller if the correlation is not significant at 99% level (we used a higher level of significance compared to Table 4 because we are dealing with the best regression of each station among the different seasons). The colors denote during which season the maximum correlation between DTR and SSR was reached (green, spring; red, summer; orange, autumn; blue, winter). Along a transect (see arrow in Figure 5a) from north to south-southwest the colored symbols build belt-like patterns, beginning with the highest-correlation coefficients occurring in the summer season in the most northern belt, which consists of the British Isles, Benelux, northern Germany and Scandinavia (Figure 5, red circles). Highest-correlation coefficients in autumn occur in the area of western France, southern Germany, the Czech Republic and eastern Poland (Figure 5, orange triangles). This second belt is followed by the most southern belt which is a mixture of springtime (Figure 5, green diamonds) and winter (Figure 5, blue squares) seasons with maximum correlation coefficients occurring around the Mediterranean and spanning the Balkan States from Hungary to the Ukraine in the east.

[47] High correlation coefficients between DTR and SSR in each pair as well as in the overall mean series for Europe are dependent on the agreement in the long-term trend behavior and the interannual variability. The interannual variability of both SSR and DTR is determined by the large-scale circulation causing high variability in cloud cover and precipitation. One of the most important features of climate in the European area is the influence of synoptic-scale pressure systems. The trajectory along which they are moving and their region of origin are related to the position of the polar front, which again is dependant on the annual orbit of the earth around the sun. Figure 5a shows that the correlation between DTR and SSR is highly dependent on the interannual variability in cloud coverage or absence due to large-scale circulation, because it mirrors the position of the polar front in the different seasons. During summer it is located northward, and with decreasing zenith angle toward autumn it moves southward together with the main trajectories of the low-pressure systems. During the winter season, the dynamic low-pressure systems can reach as far south as the Mediterranean and as far east as the Black Sea, while causing interannual variability in SSR via alteration of cloud coverage. With the increasing zenith angle the polar front moves northward again causing the highest-correlation coefficients of all seasons in the Balkan States, Hungary and southwestern France. If still we claim the interannual variability of synoptic-scale pressure systems to be of utmost importance for the highest correlation between DTR and SSR on a seasonal and interannual scale, long-term behavior of SSR and DTR are not only dependent on clouds or cloud absence but also on transmissivity of the atmosphere which is determined by the aerosol burden of the atmosphere. *Norris and Wild* [2007] show that removing the cloud effect from SSR emphasizes the dimming and brightening trend which we also identified in the European mean series of DTR and SSR (Figure 3).

[48] From the correlations of the long-term variations no distinct pattern is apparent. Most prominent, however, is the cluster of the highest winter maximum correlations east of 10°E and summer maxima north of 55°N (Figure 5b). This pattern might be due to the Siberian High, which causes persistent clear sky situations. Long-term, changes in SSR consequently may have left their fingerprint here most prominently. The fact that the strongest correlations between DTR and SSR in northern Europe appear during the summer season (in the long-term as well as in the short-term variations) is rather little surprising, since during this period SSR is largest and can drive DTR effectively.

5. Modeling DTR and SSR

[49] In this section we assess the representation of SSR and DTR and most importantly their relationship to each other and the measurements in different Regional Climate Models (RCMs) simulations from the ENSEMBLES project. The purpose of this section is to assess the usefulness of RCMs to better understand the various physical mechanisms governing to relationship between DTR and SSR by analyzing how realistic the model output is.

[50] For the comparison of our station data sets against model output we use nine different models which all performed simulations for the same region and for the same boundary conditions, using ERA40 reanalysis data, with 0.22° (25 km) resolution. For two of the nine different model versions we analyzed additional simulations at coarser resolution (0.44°/50 km). More detailed information on the selected simulations can be found in section 2.3. As previously mentioned, we use the institution name combined with "22" or "44," representing the resolution of

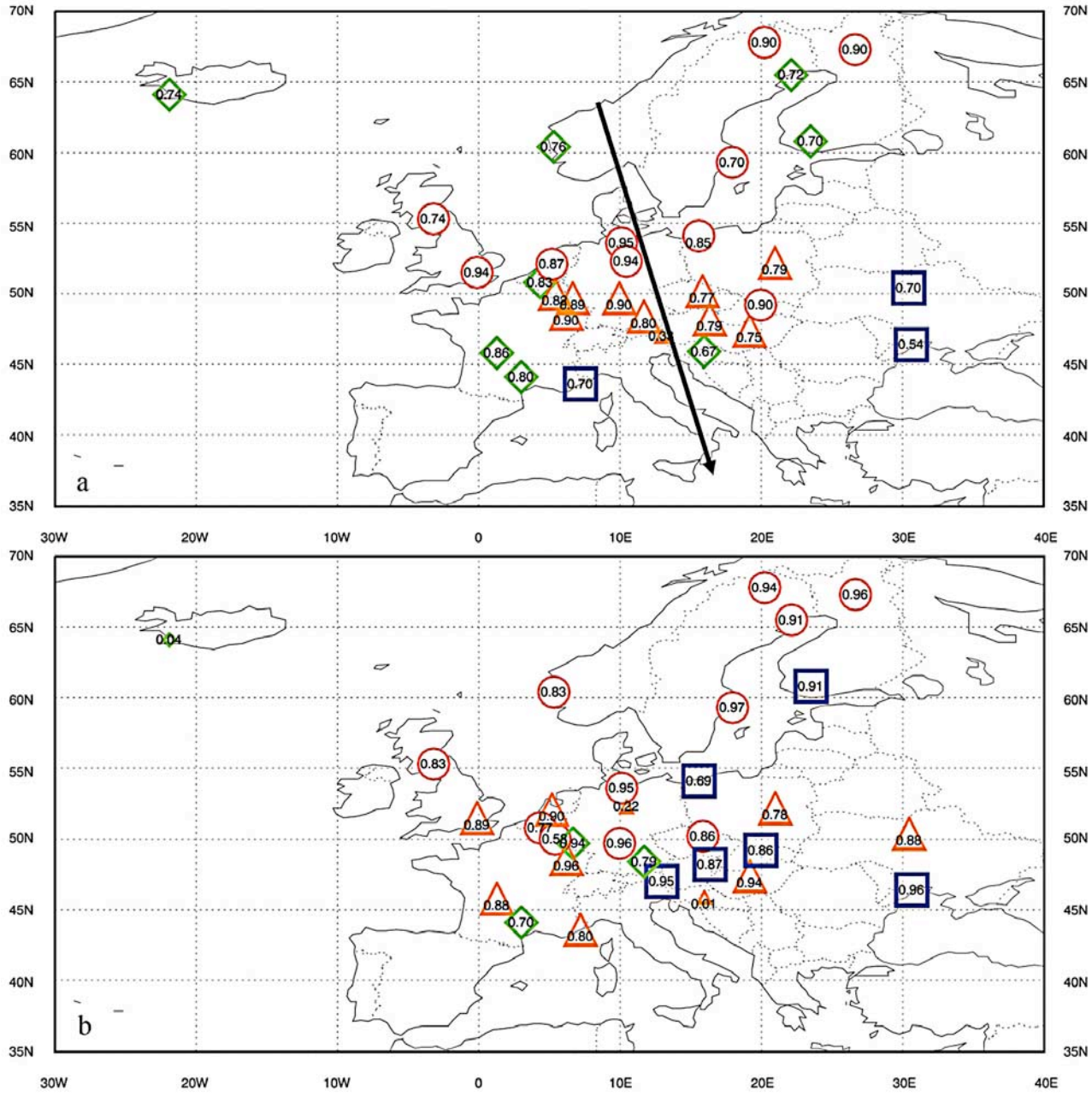

Figure 5. Map of the seasons with highest correlation in the detrended, (a) short-term and (b) long-term variations for each pair of stations. Symbols contain the corresponding correlation coefficient. Smaller symbols denote correlations not significant at the 99% level. Highest correlation of all seasons between diurnal temperature range (DTR) and surface solar radiation (SSR) is denoted by red circles in summer, orange triangles in autumn, green diamonds in spring, and blue squares in winter. Arrow indicates pattern transect as defined in the text.

0.22°/25 km or 0.44°/50 km respectively, to unambiguously refer to a model version (Table 2).

5.1. Modeled DTR and SSR in the ENSEMBLES RCMs

[51] From the monthly mean output of the models we derived annual and seasonal mean values for each year between 1970 and 2000 using the same definitions of seasons as for the station data. In Table 5 we summarized the results from the correlation calculation between detrended modeled DTR and SSR. For comparison we added the correlation coefficients as derived from the station data sets in Table 5. To ensure an appropriate comparison we recalculated all correlation coefficients between measured DTR and SSR for the period 1970–2000.

[52] In general we found the highest-correlation coefficients between DTR and SSR in spring and summer in the models. The mean of all correlation coefficients in spring

Table 5. Correlation Coefficients of Diurnal Temperature Range and Surface Solar Radiation in Each Simulation and in the First Two Lines for Comparison of the Measurements for the Periods 1970–2005 and 1970–2000[a]

	Spring	Summer	Autumn	Winter	Annual
Station data 1970–2005	**0.88**	**0.92**	**0.88**	**0.61**	**0.87**
Station data 1970–2999	**0.86**	**0.92**	**0.89**	**0.68**	**0.82**
C4I22	**0.90**	**0.84**	**0.83**	**0.61**	**0.89**
CNRM22	**0.92**	**0.87**	**0.85**	**0.71**	**0.81**
DMI22	**0.93**	**0.94**	**0.83**	**0.66**	**0.72**
ETHZ22	**0.87**	**0.96**	**0.92**	**0.68**	**0.90**
ETHZ44	**0.87**	**0.91**	**0.90**	**0.72**	**0.89**
ICTP22	**0.94**	**0.93**	**0.88**	**0.57**	**0.86**
KNMI22	**0.87**	**0.95**	**0.89**	**0.68**	**0.85**
KNM144	**0.87**	**0.93**	**0.89**	**0.74**	**0.82**
MPI22	**0.92**	**0.87**	**0.85**	0.16	**0.74**
OURANOS22	**0.94**	**0.92**	**0.92**	**0.70**	**0.84**
SMHI22	**0.91**	**0.88**	**0.87**	**0.67**	**0.90**
Model mean	0.90	0.91	0.88	0.63	0.84

[a]Bold numbers are significant at the 99% level.

and summer is 0.90 and 0.91, respectively (Table 5, model mean row). These values are very similar to the measurement correlation coefficients, namely 0.86 for spring and 0.93 for the summer season (Table 5, row 2). The coefficients of the winter season are generally lowest, analogous to the measurement data analysis. They range from 0.50 to 0.75 (measurement data analysis: 0.67) except for one outlier with 0.41 (MPI22). The mean of the annual mean correlation coefficients of all models is 0.87, which falls in between the measurement correlation coefficients, namely 0.86 (1970–2000) and 0.89 (1970–2005).

[53] The low-frequency variability (not shown) of DTR and SSR agrees well in all models and seasons with positive significant correlations values ranging from 0.54 to 1.00 except for two outliners which were identified in the winter mean of MPI22 (−0.40) and the annual mean of DMI22 (0.32).

[54] To summarize, we can state that the internal correlations between modeled DTR and SSR are very similar to the correlations of measured DTR and SSR in both seasonal and annual averages. When comparing the course of the seasons, most simulations reproduced internally realistic correlation coefficients, from midcorrelation to high-correlation coefficients in spring and summer to midcorrelation and low-correlation coefficients in autumn and winter.

5.2. Verification of Modeled Time Series of European DTR and SSR

[55] We use all simulations forced by ERA40 boundary conditions and analyzed for the period 1970–2000. To analyze their temporal performance the measured DTR is compared to the modeled DTR (Table 6) and the measured SSR to the modeled SSR (Table 7). Once again we have split the time series into their low- and high-frequency part by applying a Lowess algorithm [*Cleveland*, 1979].

[56] The highest-correlation coefficients (Tables 6 and 7, indicated with footnotes) in spring, summer and autumn in both DTR and SSR high-frequency variability are found in both the ETHZ22 or the ETHZ44. For the winter period the best performance for the high variability part of SSR time series is found in KNMI44. Also with respect to DTR, KNMI44 performs well. However, the best representation of model DTR (detrended) could be found in the DMI22 and C4I22. The lowest-correlation coefficients between modeled and measured high-frequency variability (Tables 6 and 7, indicated with footnotes) for nearly all seasons in DTR and SSR are found in CNRM22.

[57] The low-frequency variations of DTR and SSR are compiled in the right-hand side (columns 7–11) of Tables 6 and 7. It is most striking that all models reproduce the long-term variation during winter and especially autumn quite well. The finding that all models perform equally well indicates that the prescribed ERA40 boundary conditions are likely causing this agreement. This suggests that not only the high-frequency changes during autumn and winter are influenced by large-scale circulation but also the long-term fluctuations.

[58] It is further noteworthy that in the mean of all simulations the summer season series of both DTR and SSR were reproduced worst of all seasons in the low- and high-frequency part. *Jacob et al.* [2007] and *Jaeger et al.* [2008] discuss the weak RCM performance in summer and attributed it to the increased importance of small-scale

Table 6. Same as Table 5 but for Measured Compared With Modeled Diurnal Temperature Range[a]

	Coefficients of Detrended Time Series Residuals					Coefficients of the Low-Frequency, Long-Term Variability of the Time Series[b]				
	Spring	Summer	Autumn	Winter	Annual	Spring	Summer	Autumn	Winter	Annual
C4I22	**0.67**	0.42	**0.69**	**0.65**[c]	**0.55**	−0.34	0.19	**0.77**	**0.89**	−0.41[d]
CNRM22	0.41[d]	**0.48**	**0.66**[d]	0.37[d]	**0.57**	**0.54**[d]	0.24	**0.65**[d]	0.18	0.17
DMI22	**0.78**	**0.64**	**0.79**	**0.65**[c]	**0.53**	0.24	**0.64**	**0.78**	**0.85**	−0.36
ETHZ22	**0.83**[c]	**0.78**	**0.84**[c]	**0.58**	**0.87**[c]	**0.51**	**0.60**	**0.91**	**0.96**	0.36
ETHZ44	**0.82**	**0.80**[c]	**0.80**	**0.60**	**0.83**	**0.65**[c]	**0.75**[c]	**0.83**	**0.98**[c]	0.44[c]
ICTP22	**0.64**	0.41	**0.76**	**0.59**	**0.51**	**0.62**	**0.54**	**0.92**[c]	**0.98**[c]	0.12
KNMI22	**0.80**	0.30[d]	**0.73**	**0.63**	**0.64**	0.09	−0.12	**0.87**	**0.98**	−0.32
KNMI44	**0.73**	**0.47**	**0.74**	**0.64**	**0.65**	0.15	−0.16[d]	**0.84**	**0.97**	−0.27
MPI22	**0.76**	**0.65**	**0.69**	**0.64**	**0.67**	**0.54**	0.40	**0.88**	**0.86**	−0.11
OURANOS22	**0.63**	0.34	**0.68**	0.39	0.43[d]	0.10	−0.02	**0.90**	0.17[d]	−0.26
SMHI22	**0.67**	**0.50**	**0.75**	**0.55**	**0.54**	−0.38	0.18	**0.76**	**0.93**	−0.17
Model Mean	0.70	0.53	0.74	0.57	0.62	0.15	0.30	0.83	0.80	−0.07

[a]Bold coefficients are significant at the 99% level.
[b]Determined with Lowess algorithm.
[c]Highest-correlation coefficients of all simulations in each period.
[d]Lowest-correlation coefficients of all simulations in each period.

Table 7. Same as Table 6 but for Surface Solar Radiation[a]

	Coefficients of Detrended Time Series Residuals					Coefficients of the Low-Frequency, Long-Term Variability of the Time Series[b]				
	Spring	Summer	Autumn	Winter	Annual	Spring	Summer	Autumn	Winter	Annual
C4I22	**0.72**	**0.52**	**0.64**	**0.60**	**0.61**	**−0.62**	0.26	**0.86**	**0.81**	**−0.76**
CNRM22	0.40[c]	0.34[c]	**0.60**[c]	0.39[c]	**0.49**	−0.43	0.17	**0.79**	−0.05[c]	0.13
DMI22	**0.77**	**0.78**	**0.76**	**0.67**	**0.79**	−0.28	0.75[d]	**0.95**	**0.49**	−0.08
ETHZ22	**0.78**	**0.83**[d]	**0.83**[d]	**0.68**	**0.83**[d]	−0.18	0.40	**0.82**	**0.90**[d]	−0.37
ETHZ44	**0.79**[d]	**0.83**[d]	**0.83**[d]	**0.68**	**0.83**[d]	−0.18	0.40	**0.82**	**0.90**[d]	−0.37
ICTP22	**0.74**	**0.61**	**0.68**	**0.56**	**0.47**	0.37[d]	**0.50**	**0.98**[d]	**0.75**	−0.23
KNMI22	**0.75**	0.35	**0.72**	**0.78**[d]	0.44[c]	−0.27	−0.16[c]	**0.68**	**0.75**	**0.85**[c]
KNMI44	**0.75**	0.45	**0.76**	**0.78**[d]	**0.55**	−0.17	−0.09	**0.59**	**0.79**	**−0.77**
MPI22	**0.76**	**0.61**	**0.63**	**0.59**	**0.61**	0.35	0.39	**0.95**	0.08	−0.08
OURANOS22	**0.68**	**0.56**	**0.72**	**0.58**	**0.48**	0.35	0.41	**0.90**	0.27	0.23[d]
SMHI22	**0.74**	**0.64**	**0.75**	**0.67**	**0.61**	**0.69**[c]	−0.06	**0.86**	**0.88**	**−0.72**
Model mean	0.72	0.59	0.72	0.63	0.60	−0.14	0.26	0.81	0.59	−0.35

[a]Bold coefficients are significant at the 99% level.
[b]Determined with Lowess algorithm.
[c]Lowest-correlation coefficients of all simulations in each period.
[d]Highest-correlation coefficients of all simulations in each period.

processes such as convection or land-atmosphere interactions for the regional European summer climate, in contrast to the predominance of the large-scale circulation for the winter climate.

[59] Since aerosols were included as climatology only, the missing agreement between modeled and measured time series of DTR and SSR during the higher-insolation seasons of the year might also be an indication of the importance of the influence of scattering and absorbing aerosols which changed substantially during the second half of the 20th century [*Mylona*, 1996; *Lefohn et al.*, 1999; *Vestreng et al.*, 2007] thus altering the SSR [*Marmer et al.*, 2007] and consequently the DTR [*Makowski et al.*, 2008].

5.3. Modeled Relationship Versus Measured Relationship of DTR and SSR

[60] In addition to assessing the reliability of the model-internal correlations and the long- and short-term time series behavior of DTR and SSR, we also investigated the absolute values compared to the different seasons in the measurement data sets. In Figure 6 we compiled all scatterplots of all model versions and compared them to the station measurement data, which are as we have shown in section 3.3 representative for the entire European domain. Each panel of Figure 6 contains all scatterplots for the four seasons and the annual mean of measured DTR against measured SSR (gray) and modeled DTR against modeled SSR (black). The measured and modeled seasons are connected with one line each. The dotted line connects winter (Figure 6, bottom left), autumn, spring and summer (Figure 6, top right) of the station data sets, and the solid line connects those of the simulations. The anchor points for the connecting lines are the arithmetic means of both measures for each season. The dashed lines connect each plotted season of the measurements with the corresponding season of the model simulation. The scatterplot of the annual mean (Figure 6, gray and black, cross) is always located in the middle of the five different black or gray scatterplots.

[61] From the dotted line in Figure 6, which connects the measured data, one can see a homogeneous picture of increasing DTR and SSR. Highest values occur during the season with the highest zenith angle, and lowest values with the lowest zenith angle. This is not reproduced in each of the 11 model simulations however. The most striking feature while comparing the modeled data against the measured data is the fact that 8 out of 11 model simulations underestimate either DTR or SSR or both. The dashed lines (black) in each scatterplot of Figure 6 connect the means of the corresponding season and indicate the type of overall error. If they are more or less vertical (C4I22, DMI22), then DTR is either under or overestimated, if they are more horizontally oriented they point toward an under or overestimation of SSR. If the dashed lines are "parallel" to the potential regression lines (ETHZ22/44, KNMI22/44, MPI22) of each season's scatterplot then they indicate a systematic low or high bias in both DTR and SSR. In general, Figure 6 panels with parallel dashed lines for the different seasons show the simulations with a systematic bias, whereas panels with dashed lines which point in completely different directions identify potentially more complex and seasonally different errors.

[62] A further two weaknesses are obvious from the comparison of the 9 model versions with the measured data. First, the simulations C4I22, DMI22, OURANOS22 and SMHI22 all show that, either winter and summer are too low or spring and autumn are too high in the internal comparison (Figures 6a, 6c, 6j, and 6k). Second, when looking additionally at CNRM22 and ETHZ22/44 (Figures 6b, 6d, and 6e) it is clear that the summer period seems to be the most difficult to reproduce correctly for the models.

[63] ETHZ22/44 and KNMI22/44 (Figures 6d and 6e and Figures 6g and 6h) represent two pairs of simulations that have been run with the same model setup but different horizontal resolutions. We found the same systematic deficiencies compared to the measured data, but a stronger low bias in the coarse resolution simulations.

6. Summary and Conclusions

[64] This study provides evidence for a strong connection between SSR and DTR on annual scale and in different seasons in both observations and Regional Climate Model

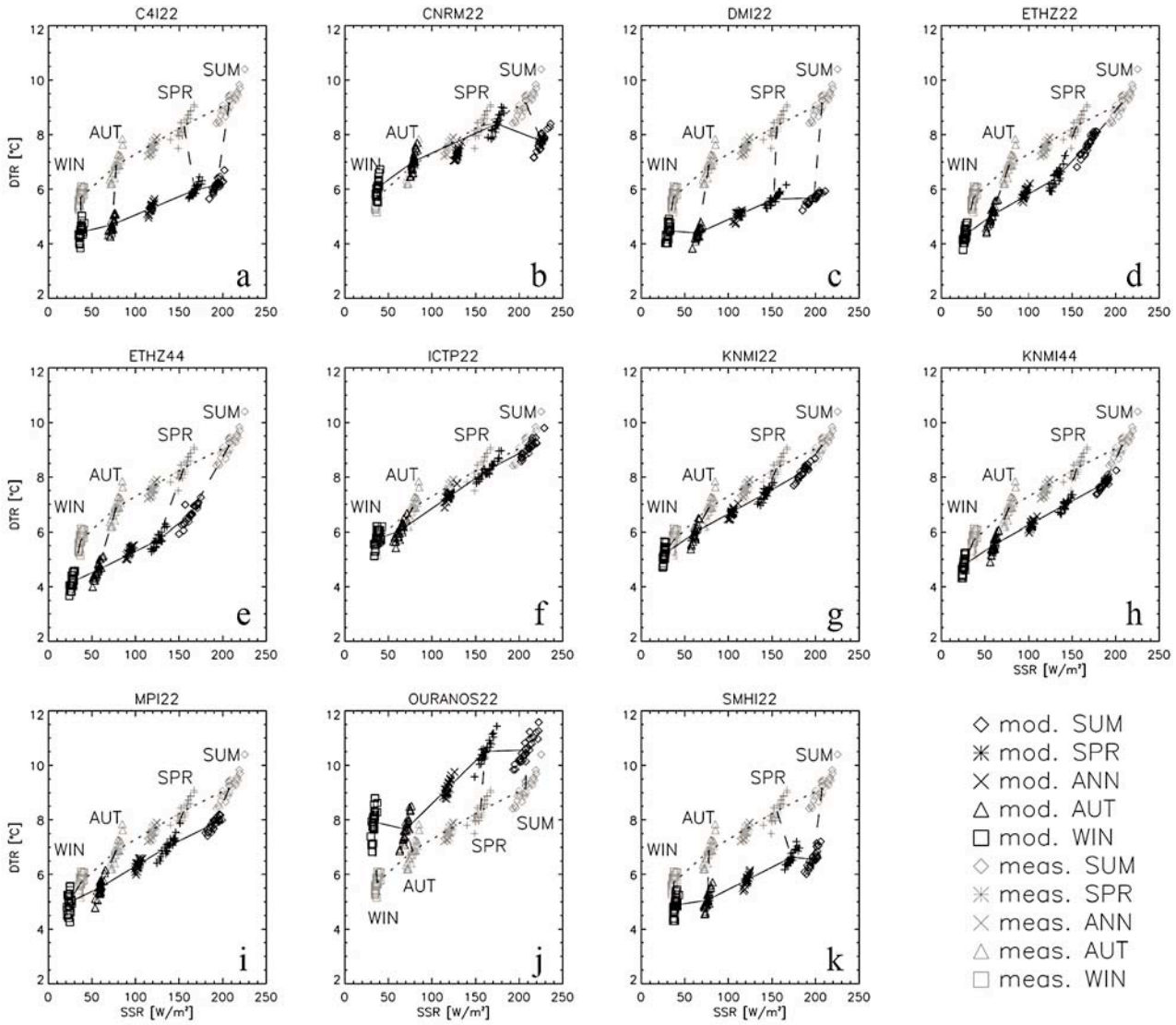

Figure 6. Scatterplots of diurnal temperature range (DTR) and surface solar radiation (SSR) anomalies. Scatterplots of measured station data set are the same in each panel and given as a reference (gray). The seasons are connected with a dotted line and labeled with WIN for winter, AUT for autumn, SPR for spring, and SUM for summer. Fifth unlabeled scatter cloud in each color (black or gray) represents the annual mean. The symbols representing each season and the annual mean are given in the legend. Dashed lines connect the corresponding seasons of measured (meas.) and modeled (mods.) data. Modeled data are given in black. The solid line connects the different seasons.

simulations. In the annual mean anomalies the correlation is 0.86 for the period 1970–2005. On the seasonal scale the detrended summer season shows the highest correlations in the measurements (0.92) and the models (0.91) followed by spring (0.88/0.90 measurements/models), autumn (0.88/0.88) and winter (0.61/0.63). We also show that the DTR anomaly series which we derived from a set of 31 carefully selected sites represents the major characteristics of the entire European domain as seen in ECAD and CRU gridded data sets; this applies for the high- and low-frequency component of the time series.

[65] The multidecadal evolution of the annual mean DTR time series over the complete period from 1970 to 2005, if still not significant at the 95% level, follows that of the SSR series, which once more shows the well known behavior of decrease and increase, also termed global dimming and brightening. The dimming and brightening is most evident in the annual mean and the summer and autumn season, with trends significant at the 95% level.

[66] An assessment of the highest correlated season for each pair of a DTR and an SSR site showed that synoptic-scale pressure systems likely have a strong influence on the interannual variability, contributing to the reported high correlation between DTR and SSR.

[67] The comparison of the observed relationships with their counterparts in the current generation regional climate models revealed several major issues. In most models the seasonal correlation coefficients and their changing behavior in the annual cycle (highest summer, lowest winter) are

correctly reproduced and of comparable magnitude as in the measurements.

[68] By comparing absolute values of DTR and SSR from measurements and models we found that more than 50% of the simulations analyzed produced, in general, too low values in DTR and SSR. The seasons often do not have the right relationship compared with each other; we found, for example, summer seasons with lower mean SSR than the mean of the spring season of the same model.

[69] When comparing the measured time series of DTR and SSR against the model DTR and SSR we found that the interannual variation of DTR and SSR is reproduced fairly well with correlation coefficients mostly between 0.5 and 0.8. It is noteworthy that on average the short- and long-term variability of the summer season were reproduced worst, despite the fact that the simulations were all driven by ERA40 reanalysis boundary conditions. This may be a result of small-scale processes being poorly resolved in the models, particularly since these processes play an important role in summer. Aerosol influence may also be responsible since their concentrations are determined from a climatology rather than from actual values. The lacking time dependence of atmospheric aerosol burden might explain the missing long-term temporal change of SSR and DTR, especially in the summer season. In contrast, the autumn period reproduced realistic results in the short-term and even more in the long-term development. This may be interpreted as an indication for the strong influence of the large-scale circulation on the long-term behavior of DTR and SSR during the period of the year when incident angles are low.

[70] From these results we conclude that DTR and SSR in Europe are strongly interconnected and influenced by the same factors. The connection is stronger on seasonal scales than on the annual scale. The agreement on the level of interannual variability is high and robust which shows the strong influence of large-scale circulation and cloud coverage. We consider it possible to estimate seasonal and interannual variability of SSR from DTR data in Europe. Concerning the long-term development of SSR, the presented findings encourage us that we may be able to estimate SSR from DTR, however longer and carefully homogenized time series are needed for this purpose and other factors, such as the role of air and soil moisture, need to be better quantified.

[71] **Acknowledgments.** We acknowledge the EU-FP6 project ENSEMBLES (http://www.ensembles-eu.org) for access to the RCM simulations and to the gridded observational data set. We are indebted to the data provided in the ECAD project (http://eca.knmi.nl) and the Climate Research Unit of the University of East Anglia. Discussions with Thomas Peter, Doris Folini, and Jörg Mäder were highly appreciated. The comments of Binhui Liu and a second anonymous reviewer helped to improve this work substantially. The work was funded by ETH Zurich, Polyproject: "Variability of the sun and global climate" – Phase II, with contributions of NCCR Climate funded by the Swiss National Science Foundation.

References

ALADIN International Team (1997), The ALADIN Project: Mesoscale modelling seen as a basic tool for weather forecasting and atmospheric research, *WMO Bull.*, *46*(4), 317–324.

Bristow, K. L., and G. S. Campbell (1984), On the relationship between incoming solar radiation and daily maximum and minimum temperature, *Agric. For. Meteorol.*, *31*(2), 159–166, doi:10.1016/0168-1923(84)90017-0.

Christensen, J. H., O. Bossing Christensen, P. Lopez, E. Van Meijgaard, and M. Botzet (1996), The HIRHAM4 Regional Atmospheric Climate Model, *DMI Sci. Rep. 96–4*, Dan. Meteorol. Inst., Copenhagen.

Cleveland, W. S. (1979), Robust locally weighted regression and smoothing scatterplots, *J. Am. Stat. Assoc.*, *74*(368), 829–836, doi:10.2307/2286407.

Dai, A., A. D. DelGenio, and I. Y. Fung (1997), Clouds, precipitation and temperature range, *Nature*, *386*(6626), 665–666, doi:10.1038/386665b0.

Easterling, D. R., et al. (1997), Maximum and minimum temperature trends for the globe, *Science*, *277*(5324), 364–367, doi:10.1126/science.277.5324.364.

Gilgen, H., and A. Ohmura (1999), The Global Energy Balance Archive, *Bull. Am. Meteorol. Soc.*, *80*(5), 831–850, doi:10.1175/1520-0477(1999)080<0831:TGEBA>2.0.CO;2.

Giorgi, F., and L. O. Mearns (1999), Introduction to special section: Regional climate modeling revisited, *J. Geophys. Res.*, *104*(D6), 6335–6352, doi:10.1029/98JD02072.

Haylock, M. R., N. Hofstra, A. M. G. Klein Tank, E. J. Klok, P. D. Jones, and M. New (2008), A European daily high-resolution gridded dataset of surface temperature and precipitation for 1950–2006, *J. Geophys. Res.*, *113*, D20119, doi:10.1029/2008JD010201.

Jacob, D., et al. (2001), A comprehensive model inter-comparison study investigating the water budget during the BALTEX-PIDCAP period, *Meteorol. Atmos. Phys.*, *77*(1–4), 19–43, doi:10.1007/s007030170015.

Jacob, D., et al. (2007), An inter-comparison of regional climate models for Europe: Model performance in present-day climate, *Clim. Change*, *81*, 31–52, doi:10.1007/s10584-006-9213-4.

Jaeger, E., I. Anders, D. Lüthi, B. Rockel, C. Schär, and S. I. Seneviratne (2008), Analysis of ERA40-driven CLM simulations for Europe, *Meteorol. Z.*, *17*(4), 349–367.

Jones, C. G., U. Willen, A. Ullerstig, and U. Hansson (2004), The Rossby Centre Regional Atmospheric Climate Model part 1: Model climatology and performance for the present climate over Europe, *Ambio*, *33*(4–5), 199–210, doi:10.1639/0044-7447(2004)033[0199:TRCRAC]2.0.CO;2.

Jones, P. D. (1995), Maximum and minimum temperature trends in Ireland, Italy, Thailand, Turkey and Bangladesh, *Atmos. Res.*, *37*(1–3), 67–78, doi:10.1016/0169-8095(94)00069-P.

Karl, T. R., G. Kukla, and J. Gavin (1984), Decreasing diurnal temperature range in the United States and Canada from 1941 through 1980, *J. Clim. Appl. Meteorol.*, *23*(11), 1489–1504, doi:10.1175/1520-0450(1984)023<1489:DDTRIT>2.0.CO;2.

Karl, T. R., G. Kukla, V. N. Razuvayev, M. J. Changery, R. G. Quayle, R. R. Heim, D. R. Easterling, and C. B. Fu (1991), Global warming: Evidence for asymmetric diurnal temperature change, *Geophys. Res. Lett.*, *18*(12), 2253–2256, doi:10.1029/91GL02900.

Karl, T. R., P. D. Jones, R. W. Knight, G. Kukla, N. Plummer, V. Razuvayev, K. P. Gallo, J. Lindseay, R. J. Charlson, and T. C. Peterson (1993), A new perspective on recent global warming—Asymmetric trends of daily maximum and minimum temperature, *Bull. Am. Meteorol. Soc.*, *74*(6), 1007–1023, doi:10.1175/1520-0477(1993)074<1007:ANPORG>2.0.CO;2.

Kjellström, E., L. Bärring, S. Gollvik, U. Hansson, C. Jones, P. Samuelsson, M. Rummukainen, A. Ullerstig, U. Willén, and K. Wyser (2005), A 140-year simulation of European climate with the new version of the Rossby Centre regional atmospheric climate model (RCA3), *Rep. Meteorol. Climatol. 108*, 54 pp., Swed. Meteorol. and Hydrol. Inst., Norrkoping, Sweden.

Klein Tank, A. M. G., et al. (2002), Daily dataset of 20th-century surface air temperature and precipitation series for the European Climate Assessment, *Int. J. Climatol.*, *22*(12), 1441–1453, doi:10.1002/joc.773.

Lefohn, A. S., J. D. Husar, and R. B. Husar (1999), Estimating historical anthropogenic global sulfur emission patterns for the period 1850–1990, *Atmos. Environ.*, *33*(21), 3435–3444, doi:10.1016/S1352-2310(99)00112-0.

Lenderink, G., B. J. J. M. van den Hurk, E. van Meijgaard, A. van Ulden, and J. Cuijpers (2003), Simulation of present-day climate in RACMO2: First results and model developments, *KNMI Tech. Rep. 252*, 24 pp., R. Neth. Meteorol. Inst., De Bilt, Netherlands.

Liepert, B. G. (2002), Observed reductions of surface solar radiation at sites in the United States and worldwide from 1961 to 1990, *Geophys. Res. Lett.*, *29*(10), 1421, doi:10.1029/2002GL014910.

Liu, B. H., M. Xu, M. Henderson, Y. Qi, and Y. Q. Li (2004), Taking China's temperature: Daily range, warming trends, and regional variations, 1955–2000, *J. Clim.*, *17*(22), 4453–4462, doi:10.1175/3230.1.

Makowski, K. (2006), Veränderung der maximalen und minimalen Tagestempertauren im Bereich der nördlichen Hemisphäre, M.Sc. thesis, 108 pp., Univ. Zurich, Zurich, Switzerland.

Makowski, K., M. Wild, and A. Ohmura (2008), Diurnal temperature range over Europe between 1950 and 2005, *Atmos. Chem. Phys.*, *8*(21), 6483–6498.

Marmer, E., B. Langmann, H. Fagerli, and V. Vestreng (2007), Direct shortwave radiative forcing of sulfate aerosol over Europe from 1900 to 2000, *J. Geophys. Res.*, *112*, D23S17, doi:10.1029/2006JD008037.

Mitchell, T. D., and P. D. Jones (2005), An improved method of constructing a database of monthly climate observations and associated high-resolution grids, *Int. J. Climatol.*, *25*(6), 693–712, doi:10.1002/joc.1181.

Mylona, S. (1996), Sulphur dioxide emissions in Europe 1880–1991 and their effect on sulphur concentrations and depositions, *Tellus, Ser. B*, *48*(5), 662–689, doi:10.1034/j.1600-0889.1996.t01-2-00005.x.

Norris, J. R., and M. Wild (2007), Trends in aerosol radiative effects over Europe inferred from observed cloud cover, solar "dimming," and solar "brightening", *J. Geophys. Res.*, *112*, D08214, doi:10.1029/2006JD007794.

Pal, J. S., et al. (2007), Regional climate modeling for the developing world—The ICTP RegCM3 and RegCNET, *Bull. Am. Meteorol. Soc.*, *88*(9), 1395–1409, doi:10.1175/BAMS-88-9-1395.

Pinker, R. T., B. Zhang, and E. G. Dutton (2005), Do satellites detect trends in surface solar radiation?, *Science*, *308*(5723), 850–854, doi:10.1126/science.1103159.

Plantico, M. S., T. R. Karl, G. Kukla, and J. Gavin (1990), Is recent climate change across the United-States related to rising levels of anthropogenic greenhouse gases, *J. Geophys. Res.*, *95*(D10), 16,617–16,637, doi:10.1029/JD095iD10p16617.

Plummer, D. A., D. Caya, A. Frigon, H. Cote, M. Giguere, D. Paquin, S. Biner, R. Harvey, and R. De Elia (2006), Climate and climate change over North America as simulated by the Canadian RCM, *J. Clim.*, *19*(13), 3112–3132, doi:10.1175/JCLI3769.1.

Stanhill, G., and S. Cohen (2001), Global dimming: A review of the evidence for a widespread and significant reduction in global radiation with discussion of its probable causes and possible agricultural consequences, *Agric. For. Meteorol.*, *107*(4), 255–278, doi:10.1016/S0168-1923(00)00241-0.

Steppeler, J., G. Doms, U. Schattler, H. W. Bitzer, A. Gassmann, U. Damrath, and G. Gregoric (2003), Meso-gamma scale forecasts using the nonhydrostatic model LM, *Meteorol. Atmos. Phys.*, *82*(1–4), 75–96, doi:10.1007/s00703-001-0592-9.

Teuling, A. J., et al. (2009), A regional perspective on trends in continental evaporation, *Geophys. Res. Lett.*, *36*, L02404, doi:10.1029/2008GL036584.

Uppala, S. M., et al. (2005), The ERA-40 re-analysis, *Q. J. R. Meteorol. Soc.*, *131*(612), 2961–3012, doi:10.1256/qj.04.176.

Vestreng, V., G. Myhre, H. Fagerli, S. Reis, and L. Tarrason (2007), Twenty-five years of continuous sulphur dioxide emission reduction in Europe, *Atmos. Chem. Phys.*, *7*(13), 3663–3681.

Wild, M., H. Gilgen, A. Roesch, A. Ohmura, C. N. Long, E. G. Dutton, B. Forgan, A. Kallis, V. Russak, and A. Tsvetkov (2005), From dimming to brightening: Decadal changes in solar radiation at Earth's surface, *Science*, *308*(5723), 847–850, doi:10.1126/science.1103215.

Wild, M., A. Ohmura, and K. Makowski (2007), Impact of global dimming and brightening on global warming, *Geophys. Res. Lett.*, *34*, L04702, doi:10.1029/2006GL028031.

Zhou, L. M., R. Dickinson, P. Dirmeyer, H. S. Chen, Y. J. Dai, and Y. H. Tian (2008), Asymmetric response of maximum and minimum temperatures to soil emissivity change over the Northern African Sahel in a GCM, *Geophys. Res. Lett.*, *35*, L05402, doi:10.1029/2007GL032953.

M. Chiacchio, T. Ewen, E. B. Jaeger, K. Makowski, A. Ohmura, and M. Wild, Institute for Atmospheric and Climate Science, ETH Zurich, CHN N 16.3, Universitätstrasse 16, CH-8092 Zurich, Switzerland. (makowski@env.ethz.ch)